Oral-Facial-Digital syndrome Type I cells exhibit impaired DNA repair; unanticipated consequences of defective OFD1 outside of the cilia network

Article (Accepted Version)

HMG Advance Access published October 25, 2016

Oral-Facial-Digital syndrome Type I cells exhibit impaired DNA repair; unanticipated consequences of defective OFD1 outside of the cilia network.

Iga Abramowicz[1], Gillian Carpenter[1], Mariaevelina Alfieri[2], Rita Colnaghi[1], Emily Outwin[1], Philippe Parent[3], Christel Thauvin-Robinet[4], Daniela Iaconis[2], Brunella Franco[2,5], Mark O'Driscoll[1*].

[1.] Human DNA damage Response Disorders Group, Genome Damage & Stability Centre, School of Life Sciences, University of Sussex, Falmer, Brighton, BN1 9RQ, United Kingdom.

[2.] Telethon Institute of Genetics and Medicine, Naples, Italy.

[3.] Service de Génétique, Centre Hospitalier Universitaire de Brest, France.

[4.] Centre de Génétique, Hôpital d'Enfants, 14 rue Paul Gaffarel, 21079 Dijon Cedex, France.

[5.] Department of Medical Translational Sciences, Federico II University, Naples, Italy.

***Corresponding author:** m.o-driscoll@sussex.ac.uk

Ph. 0044 (0) 1273 877 515

Fax. 0044 (0) 1273 678 121

Abstract.

Defects in *OFD1* underlie the clinically complex ciliopathy, Oral-Facial-Digital syndrome Type I (OFD Type I). Our understanding of the molecular, cellular and clinical consequences of impaired OFD1 originate from its characterised roles at the centrosome/basal body/cilia network. Nonetheless, the first described OFD1 interactors were components of the TIP60 histone acetyltransferase complex. We find that OFD1 can also localise to chromatin and its reduced expression is associated with mis-localization of TIP60 in patient-derived cell lines. TIP60 plays important roles in controlling DNA repair. OFD Type I cells exhibit reduced histone acetylation and altered chromatin dynamics in response to DNA double strand breaks (DSBs). Furthermore, reduced OFD1 impaired DSB repair via homologous recombination repair (HRR). OFD1 loss also adversely impacted upon the DSB-induced G2-M checkpoint, inducing a hypersensitive and prolonged arrest. Our findings show that OFD Type I patient cells have pronounced defects in the DSB-induced histone modification, chromatin remodelling and DSB-repair via HRR; effectively phenocopying loss of TIP60. These data extend our knowledge of the molecular and cellular consequences of impaired OFD1, demonstrating that loss of OFD1 can negatively impact upon important nuclear events; chromatin plasticity and DNA repair.

Introduction.

Oral-Facial-Digital syndrome, Type I (OFD1; OMIM 311200), belongs to a heterogeneous group of developmental conditions; the oral-facial-digital syndromes (OFDS)(1-3). OFD Type I is caused by mutations in *OFD1* (formerly *Cxorf5*) which tend to occur sporadically, segregating in an X-linked dominant fashion and causing male lethality, usually in the 1st / 2nd trimester (4, 5). Nevertheless, rare cases of male OFD Type I have been reported (2, 6, 7). Heterozygous deletion and genomic rearrangements involving *OFD1* have also been reported as disease mechanisms (8-10). OFD Type I is clinically complex and variable, yet features affecting the craniofacial region (e.g. hypertelorism, microretrognathia, epicanthis, down-slanting palpebral fissures), oral cavity (e.g. lobulated, bifid, cleft tongue, cleft and high arched palate, alveolar ridge clefting) and the skeletal system (e.g. short stature, brachydactyly, syndactyly, clinodactyly) predominate (2, 10). OFD Type I is notable for the occurrence of cystic disease, particularly in the kidneys, but also elsewhere (e.g. liver, pancreas, brain)(2). OFD Type I patients also exhibit profound neurological impacts including cognitive and behavioural abnormalities and complex structural brain abnormalities (9, 11).

OFD1 encodes a 1011 amino acid protein composed of five α helical coiled-coil domains (α-CC) and N-terminally localised LisH (Lis1 homology) domain, but lacks homology to proteins of known function (5). LisH motifs have been postulated to mediate an array of activities including cell migration, nucleokinesis, protein dimerization and transcription (12). The α-CC is a highly versatile motif mediating protein-protein interaction and subunit oligomerization (13). Nevertheless, OFD1 amino acid sequence lacks any obvious and characteristic indicators of cellular functionality. Importantly, generation of an *Ofd1* knockout mouse model established a role for Ofd1 in cilia formation and function (14). These mice recapitulated the human disorder, although with increased severity as a likely

consequence of the differing nature of X-inactivation between mouse and humans (14). *Ofd1* knockout mice exhibited marked failure in left-right axis specification, cystic kidneys and a failure to form cilia in the embryonic node (14). This was associated with defective sonic hedgehog (Shh) and canonical WNT signalling (14-16). Many of these findings have been recapitulated in other model organisms such as zebrafish (*Danio rerio*)(17). Consequently, cell biological research has primarily focused on dissecting the precise role(s) of OFD1 at the centrosome/basal body/cilium.

OFD1 can localise to the centrosome, co-localizing with γ-tubulin, but specifically to the centriolar satellite region surrounding the centrosome and basal body (18, 19). OFD1 has been shown to interact with PCM-1 (20). OFD1 regulates the length and structure of distal centrioles (21). Recently, autophagic degradation of the centriolar satellite pool of OFD1 specifically was found to be required for cilia formation, indicating a context-specific regulation of OFD1 in controlling ciliogenesis (22, 23). There now exists a compelling body of evidence demonstrating that impaired OFD1 function negatively impacts upon cilia mediated paracrine signalling from multiple pathways including Shh, WNT and NOTCH, firmly establishing OFD Type I as a ciliopathy (24).

Interestingly, OFD1 has also been shown to localise to the nucleus, suggesting it may also have additional functions outside of the centrosome/basal body/cilia (19). Furthermore, OFD1 was found to co-immunoprecipitate several components of the TIP60 histone acetyltransferase (HAT) multi-subunit complex, including DMAP1, TIP60, TRRAF and RUVBL2; interacting directly with the RUVBL1 subunit (19). HAT chromatin acetylation, including that mediated by RUVBL1/2 and TIP60 containing complexes, controls transcriptional regulation (25). Additionally, TIP60 acetyltransferase complexes have established roles in activating ATM, an apical controlling kinase of the DNA damage response (DDR), in chromatin remodelling at DNA double strand breaks (DSBs) and in

controlling DSB repair (26-35). The functional implications of OFD1's association with TIP60 complexes has not been explored hitherto. Here, using OFD Type I patient cells, we characterise the impact of reduced *OFD1* expression on several interconnected aspects of the DDR including DSB-induced histone modification, chromatin remodelling and DSB repair. We provide evidence that reduced OFD1 expression causes mis-localization of TIP60, and thereby effectively phenocopies impaired TIP60 function in the DDR. We describe several novel cellular defects in OFD Type I patient cells demonstrating that this condition is characterised by compromised DSB-induced chromatin dynamics and impaired HRR-mediated DSB repair.

Results.

TIP60 is mis-localized in OFD Type I patient fibroblasts.

Much of our understanding of OFD1 function and the consequences of its dysfunction have focused on its roles at the centrosome/basal body/cilia. Yet, one of the first described OFD1 interactors was in fact the RUVBL-TIP60 HAT complex, where it was found to directly interact with at least one constituent subunit, RUVBL1 (19). We confirmed the association between OFD1 and TIP60 following transient overexpression of FLAG-tagged OFD1 in HEK293, and then immunoprecipitating it via the FLAG-tag before blotting for captured endogenous TIP60 **(Fig 1A)**. In a complementary reciprocal approach, we showed that OFD1 was detectable following immunoprecipitation of endogenous TIP60 from HeLa cell extract **(Fig 1B)**.

It is likely that only a fraction of total cellular OFD1 interacts with TIP60, yet importantly, the functional significance of the association between OFD1 and the RUVBL-

TIP60 HAT complex has not been investigated. Using indirect immunofluorescence detection of TIP60 in OFD Type I patient fibroblasts from two separate individuals (FB.1 and FB.2), we unexpectedly observed a marked accumulation of cytoplasmic staining, in contrast to wild-type (WT) fibroblasts (**Fig 1C**). OFD: FB.1 fibroblasts, bearing a frameshift mutation in *OFD1* (1360delCTAA), are derived from an OFD Type I individual described previously (Family 4) by Christel Thauvin-Robinet and colleagues (36). OFD: FB.2 fibroblasts are derived from a previously unreported patient with a missense variant in OFD1 (p.H81Q). This variant has been catalogued as pathogenic in ClinVar (http://www.ncbi.nlm.nih.gov/clinvar/variation/41101/). Cytoplasmic accumulation of TIP60 was also seen following siRNA knockdown of *OFD1* in WT fibroblasts indicating that reduced OFD1 is associated with a redistribution and mis-localization of TIP60 within cells (**Fig 1D**).

We next performed sub-cellular fractionation of WT and OFD: FB.2 fibroblasts followed by western blotting analysis of TIP60 levels. Interestingly, we found reduced TIP60 levels in the nuclear fraction of OFD: FB.2 fibroblasts compared to WT cells (**Fig 2A**). To further investigate the implications of these findings in the specific context of other OFD Type I patient cell type we next employed lymphoblastoid cells (LCLs) from an OFD Type I female patient with a frameshift in *OFD1* (ex3. 275-275delCT) which results in premature truncation (p.S92CfsX115). This case was recently reported as patient ID 169 by Ennio Del Giudice and colleagues (11). OFD1 was significantly reduced in these LCLs, compared to wild-type LCLs (**Fig 2B**). Residual OFD1 was detectable consistent with hemizygosity of *OFD1* in these cells. A nuclear role for OFD1 has not previously been described. Consistent with a putative nuclear function, we found significant amounts of OFD1 on chromatin of WT LCLs, in contrast to those of OFD Type I LCLs (**Fig 2C**). Similar to our observations from the patient fibroblasts, following sub-cellular fractionation of WT and OFD Type I LCLs

followed by analysis of TIP60 expression, we found reduced TIP60 levels in the nuclear fraction of OFD Type I LCLs compared to WT cells (**Fig 2D**). Upon further fractionation of these cells we found reduced TIP60 levels in chromatin preparations of OFD Type I LCLs compared to WT **(Fig 2E).** Finally, we found that stable lentiviral shRNA knockdown of *OFD1* in U2OS resulted in reduced TIP60 in chromatin preparations (**Fig 2F**). Collectively, these findings (**Fig 1C,D and Fig 2C-F**) indicate that reduced OFD1 is associated with a subcellular redistribution of TIP60 and suggest that TIP60 functionality could be compromised through mis-localization in this context. Importantly, altered TIP60 distribution in the context of reduced OFD1 levels was observed in proliferating non-ciliated cells.

OFD Type I patient cells exhibit impaired TIP60 HAT activity and DSB-induced histone modification.

ATM activation at DSBs induces a complex series of events involving a range of histone modifications including phosphorylation, acetylation and ubiquitination. This enables the ordered recruitment of various signal transduction, chromatin remodelling and repair factors to enact effective repair (37). TIP60 plays key roles at several levels in these processes; its HAT function is activated by DSBs, TIP60 activates ATM via direct acetylation, and TIP60 acetylates specific histones facilitating chromatin remodelling and transcriptional regulation (28,31,38-40).

We observed reduced IR-induced ATM-dependent phosphorylation of several DDR factors in OFD Type I patient LCLs, although the impacts upon ATM autophosphorylation were modest (**Suppl Fig 1**). Interestingly, we observed a marked reduction in IR-induced acetylation of histone H2A on lysine-5 (H2A-AcK5) in OFD Type I fibroblasts compared to WT (**Fig 3A**). H2A-AcK5 is a TIP60-dependent acetylation (41). TIP60 also regulates DSB-

induced ubiquitination of histone H2AX, an event requiring prior acetylation (39). We observed only a modest decrease in IR-induced H2AX in OFD Type I patient fibroblasts (**Fig 3A**). This is not unexpected considering other kinases can, redundantly with ATM, conduct this phosphorylation (42). Nonetheless, we did observe reduced levels of slower migrating γH2AX species (modified; *Mod*-γH2AX), consistent with impaired IR-induced post-translational modification (e.g. ubiquitinated, acetylated and phosphorylated) of γH2AX (*Mod*-γH2AX) in OFD Type I fibroblasts, compared to WT (**Fig 3A)**. Furthermore, siRNA mediated knockdown of either *OFD1* or *TIP60* in control fibroblasts recapitulated the reduced IR-induced H2A-AcK5 and *Mod*-γ-H2AX seen in the OFD1 Type I patient fibroblasts (**Fig 3B**).

Acetylation of histone H4 on K16 plays roles in transcriptional activation, maintenance of euchromatin and in controlling higher order chromatin structure (43, 44). Several HAT complexes can acetylate histone H4 on K16 (45). Notable amongst these are MOF (MYST1/KAT8) containing HATs, which have also been implicated in the ATM-dependent DNA damage response (DDR) (46-48). DSB-induced acetylation of histone H4 on lysine-16 (H4-AcK16) has recently been shown to be an important TIP60-dependent event directing DSB repair (30). Using WT fibroblasts, we observed a transient time-dependent increase in H4-AcK16 levels up to 15mins following irradiation (**Fig 3C**). Importantly, this was in contrast to the rather unresponsive H4-AcK16 levels observed in OFD Type I fibroblasts (**Fig 3C**). Further, siRNA mediated knockdown of *OFD1* in U2OS cells similarly affected DSB-induced H4-AcK16 as observed in the patient fibroblasts (**Fig 3D**). Interestingly, siRNA of *TIP60* completely inhibited H4-AcK16 acetylation under these conditions, likely indicating that the negative impact of reduced OFD1 upon TIP60 function is not absolute, in this case. Nonetheless, these findings show that reduced OFD1 expression results in a detectable impairment of DSB-induced histone modification, including two

TIP60-dependent histone acetylation events; H2A-AcK5 and H4-AcK16 formation. Importantly, these defects are also observed in OFD Type I patient-derived cells.

OFD Type I fibroblasts exhibit impaired chromatin remodelling.

Localised chromatin remodelling at DSBs, including histone eviction and variant histone exchange are required for optimal repair (37, 49-53). Histone H4-AcK16 specifically, has been shown to control higher order chromatin structure, even impairing the action of the ACF nucleosome re-modeller in mobilizing mononucleosomes (54). DSB-induced chromatin relaxation as a consequence of enhanced histone dynamics can be assessed by monitoring the kinetics of micrococcal nuclease (MNase) digestion of chromatin (55). We undertook a modified version of this approach using a bioanalyser rather than agarose gel electrophoresis to monitor the appearance of fully digested chromatin down to mononucleosomes (**Fig 4A**). The rate of appearance of mononucleosomes was not obviously different between unperturbed untreated (Unt) WT and OFD Type I fibroblasts (**Fig 4A: Unt**). Strikingly, MNase digestion to mononucleosomes following treatment with the radiomimetic DSB-inducing agent neocarzinostatin was impaired in OFD Type I patient fibroblast compared to WT (**Fig 4A: Neo and Fig 4B**). These results are consistent with reduced chromatin plasticity/relaxation potential following DSB formation in OFD Type I fibroblasts. These data are also consistent with the altered DSB-induced histone modifications described in **Fig 3**. Furthermore, we obtained a similar attenuation of MNase accessibility after neocarzinostatin treatment following stable lentiviral mediated shRNA knockdown of *OFD1* in U2OS cells, compared to control cells (**Fig 4C-D**).

Reduced OFD1 expression impairs DSB-induced Homologous Recombination Repair.

Considering the abnormalities in DSB-induced histone modification and chromatin plasticity we observed, we next examined DSB repair capability in the context of reduced OFD1 expression. We monitored the repair of IR-induced DSBs using 53BP1 foci formation and disappearance overtime. In G_0 cells we found DSB repair to be unaffected in fibroblasts from two distinct OFD Type I patients compared to those of WT, consistent with functional non-homologous end-joining (NHEJ)-mediated DSB repair **(Fig 5A).**

TIP60 HAT complexes are directly implicated in the repair of DSBs via the Homologous Recombination Repair (HRR) pathway (29,30,34,35,56). There has been a lot of interest in dissecting the signalling networks that control DSB repair pathway choice between NHEJ and HRR. Active competition between BRCA1 and 53BP1 influence DSB end resection, determining whether repair proceeds via NHEJ (53BP1-route) or HRR (BRCA1-route) (57-61). TIP60 has recently been shown to be a key determinant of the balance between BRCA1 and 53BP1 here, whereby loss of TIP60 acetyltransferase activity reduces recruitment of BRCA1 to DSBs, impairs HRR and confers sensitivity to poly(ADP-ribosome) polymerase (PARP) (30).

DSB repair in G2 cells, when a sister chromatid template is available, can occur by HRR. We observed impaired disappearance of IR-induced 53BP1 foci in OFD Type I patient fibroblast G2 cells compared to WT, suggestive of impaired HRR **(Fig 5B).** Furthermore, we found an approximate 50% reduction in cells forming RAD51 foci following IR in OFD Type I fibroblasts compared to WT cells (**Fig 5C**). Similarly, we found lentiviral mediated shRNA of *OFD1* in U2OS cells also impaired DSB-induced RAD51 foci formation (**Fig 5D**). To directly assess HRR-mediated DSB repair capacity, we utilised the established DR-GFP reporter system based on the HRR-mediated reconstitution of an active *GFP* within an

integrated reporter cassette following I-SceI-induced DSB formation. Using this system, we found that siRNA mediated knockdown of *OFD1* resulted in ~50% reduction in HRR; a similar reduction to that observed following *TIP60* siRNA (**Fig 5E**). Together these results indicate that reduced OFD1 levels negatively affect HRR-mediated DSB repair.

The impaired HRR capacity observed following reduced OFD1 expression was associated with elevated sensitivity of OFD Type I LCLs **(Fig 6A)** and shRNA mediated knockdown of *OFD1* **(Fig 6B)** to killing by IR. Impaired HRR is synthetically lethal to inhibition of PARP using small molecule inhibitors such as olaparib (62-64). We found that OFD Type I LCLs also exhibited elevated levels of apoptosis following treatment with increasing concentrations of olaparib, as measured by the appearance of the 85 kilodalton form (p85) of caspase-cleaved PARP (**Fig 6C**). Furthermore, we observed elevated sensitivity to killing by olaparib via clonogenic assay following stable lentiviral knockdown of *OFD1* **(Fig 6D)**. Collectively, these data show that impaired OFD1 function (siRNA, shRNA), and in the context of OFD Type I patient cells, reduces DSB-induced HRR, a phenotype observed following TIP60 acetyltransferase deficiency and consistent with sub-optimal TIP60 function when OFD1 levels are reduced. These results show for the first time that reduced OFD1 expression results in impaired DNA repair in cycling non-ciliated cells.

OFD Type I LCLs exhibit a hypersensitive DSB-induced G2-M checkpoint activation and impaired recovery from arrest.

An important consequence of activation of the DDR signal transduction network is cell cycle checkpoint activation, particularly at the G2-M boundary. Unexpectedly, we found that OFD Type I LCLs exhibited a hypersensitive G2-M checkpoint activation phenotype compared to WT LCLs, showing marked G2 arrest at IR doses as low as 0.1Gy (**Fig 7A**).

Furthermore, we found that G2-M arrest was prolonged in OFD Type I LCLs compared to WT LCLs, with only approximately 30% of G2 cells progressing into mitosis 16hrs after 1Gy IR (**Fig 7B**). We observed a similar marked delay in recovery from IR-induced G2-M arrest following siRNA of *OFD1* in normal human fibroblasts, and importantly, also following siRNA of *TIP60* (**Fig 7C**). The latter observation suggests that hypersensitive and prolonged G2-M checkpoint response can occur as a consequence of impaired TIP60 acetyltransferase function and again we uncover evidence that reduced OFD1 expression mimics reduced TIP60 expression.

In summary, our data show that reduced OFD1 levels are associated with mis-localization of TIP60, and that reduced OFD1 expression results in a series of DSB-mediated histone modification, chromatin remodelling and DSB-repair deficits overlapping with those observed upon TIP60 deficiency. Furthermore, we can detect these defects in OFD Type I patient cells and under conditions independent of cilia formation (e.g. using LCLs and exponentially growing fibroblasts). Our data strongly suggest that reduced OFD1 expression can phenocopy loss of TIP60, thereby expanding our understanding of the complex consequences of impaired OFD1 function.

Discussion.

OFD Type I patients present with several core clinical features common to ciliopathies (e.g. cystic disease, patterning and limb abnormalities) (2, 65). Our understanding of the functional and clinical consequences of reduced OFD1 derive entirely from its documented roles at the centrosome/basal body/cilia network. Cilia formation and cilia-dependent paracrine signalling are markedly impaired in *Ofd1* knockout mice (14, 24, 66). Here, using patient-derived cell lines, we extend our knowledge of the cellular consequences of reduced OFD1; identifying and characterising several novel phenotypes relating to pathways controlling genomic stability, chromatin dynamics and cell cycle checkpoint control.

Whilst it is difficult to untangle the influence of the specific cellular defects described here from cilia-dependent defects in paracrine signalling, it is possible that the former may also play a contributing role to the clinical spectrum of OFD Type I syndrome. Emerging evidence suggests a growing link between congenital defects in genes encoding proteins with canonical roles in DNA repair, DDR-signalling or DNA replication and/or mitotic cell division, with impaired cilia function (67). For example, defects in components of the DNA replication licencing Origin Recognition Complex (ORC) that underlie Meier-Gorlin syndrome (MGS; a microcephalic primordial dwarfism (MPD)), were subsequently found to cause profound impairments in cilia formation and signalling; impairments which plausibly contribute to the clinical presentation of MGS (68-71). Defects in the DDR apical kinase ATR underlie another MPD; Seckel syndrome (72, 73). *Atr* deficiency was recently reported to underlie photoreceptor degeneration linked to cilia dysfunction in a mouse model of ATR-Seckel syndrome, and to negatively influence G1-S entry and Shh-signalling in ATR-Seckel fibroblasts along with altered left-right asymmetry in an *Atr* zebrafish model (74, 75). Furthermore, recent exome sequencing based searches for novel nephronophthisis-related

ciliopathy (NPHP-RC) genes identified pathogenic variants in several DNA repair and DDR-signalling proteins including FAN1, MRE11, CEP164 and ZNF432 (76, 77). Conversely, reduced expression of multiple NPHP-RC genes has been shown to induce replication stress, S phase accumulation and elevated levels of DNA damage in several model systems (78-82). Therefore, accumulating evidence indicates complex and reciprocal functional interactions between DDR, DNA Repair and cell cycle machinery with components of the cilia network. Our findings concerning OFD1 provide another layer of complexity to these relationships, where reduced OFD1 expression results in attenuated DDR signalling, DSB-induced histone modification, altered chromatin plasticity, impaired HRR and hyperactive G2 checkpoint arrest.

Disorders caused by defects in proteins with canonical roles in DDR-signalling and in DNA repair, including HRR, present a variable clinical landscape (reviewed in (83, 84)). Several interesting parallels exist between some of these conditions and OFD Type I syndrome. For example, mutations in *ATM* underlie Ataxia Telangiectasia, a progressive neurodegenerative condition characterised by progressive ataxia, ocular apraxia and dysarthria (85, 86). These motor abnormalities are characteristically observed in Joubert syndrome patients carrying *OFD1* mutations (JBTS10; OMIM 300804)(87). Structural brain abnormalities are a frequent feature of DDR-defective conditions (84). Similar abnormalities (e.g. agenesis of the corpus callosum, cerebellar hypoplasia/atrophy, cortical malformation) are also reflected in the clinical spectrum of OFD Type I patients (9, 11). Polycystic kidney disease is a characteristic feature of OFD Type I patients, often requiring dialysis and ultimately transplantation in late childhood-early adulthood (1). Interestingly, Chaki and colleagues reported the co-localisation of specific NPHP-RC proteins with TIP60 nuclear foci; and one of these NPHP-RC proteins (NPHP10/SDCCAG8) has previously been shown to directly interact with OFD1 (76, 88). Interestingly, we note that TIP60 has also recently been

identified as a constituent of the wider CPLANE (ciliogenesis and planar polarity effector) protein network (89). Collectively, these findings underscore the complex relationship between impaired DDR and normal development.

Our novel findings that reduced OFD1 expression is associated with altered DSB-induced histone modification and chromatin dynamics may have implications not just in DNA repair, but also in transcriptional regulation. These could have complex adverse impacts upon normal development via alterations of the epigenome that may also influence the clinical presentation of OFD Type I syndrome. Histone H4-AcK16, a histone post-translational modification we found to be altered in OFD Type I cells, is particularly important for the establishment and maintenance of euchromatin and in controlling higher order chromatin structure (43, 44, 54). Integrating the genome-wide distribution of this modification with the transcriptome profile of OFD Type I patient tissues may help in identifying novel abnormally regulated genes and/or networks in this context. Furthermore, altering the epigenome using various chemical inhibitors has shown therapeutic efficacy in models for other developmental disorders, such as histone deacetylase inhibitors in Kabuki syndrome (90). Whether this approach has any merit in OFD Type I models is worthy of investigation based on the histone modification abnormalities documented here.

Defects in DDR and DNA repair cause genomic instability that is often reflected as elevated cancer predisposition. Elevated cancer incidence is nonetheless not a core clinical feature of OFD Type I syndrome, although hamartomas have been described here (2). Reduced histone H4-AcK16 is a common hallmark of cancers and TIP60 is frequently under-expressed in cancer (91, 92). Importantly, these associations are complex and context specific. Loss of histone H4-AcK16 in cancer is strongly associated with coincident loss of histone H4-trimethylation at K20. Furthermore, other HATs can form H4-AcK16 and it is notable that this histone mark is not completely absent in OFD Type I patient cells (**Fig 3**). In fact, it

is perhaps even elevated above background in untreated cells compared to WT, but then unresponsive to DSBs (**Fig 3C&D**). Whilst TIP60 has been described as a tumour suppressor, *Tip60* haploinsufficiency can counteract Myc-driven lymphomagenesis in Eμ-*myc* transgenic mice (92). Our findings suggest that OFD Type I patient cells are compromised in TIP60 acetyltransferase activity likely due to subcellular mis-localization; though importantly, they are not completely defective in TIP60 function.

Finally, the novel G2-M checkpoint phenotypes we identified when OFD1 is under-expressed may be particularly relevant with regards to cancer development or lack thereof, in OFD Type I syndrome. We found a hypersensitive and prolong G2 arrest following DSB formation in OFD Type I patient cells. Compromised ATM-dependent DDR signalling is typically associated with a defective DSB arrest at G2-M. It is this defect in G2-M arrest that plays a major influence in enabling the propagation of genomic instability into malignant transformation (93). A hypersensitive G2-M checkpoint would counteract this effect, removing these cells from the cell cycle until either effective DSB repair is completed, or the cells are permanently exited from the cycling population (senescence or apoptosis) (94). Furthermore, spatio-temporal timing of mitosis is fundamental to normal cortical development (95). Embryonic brain development is associated with elevated levels of endogenous DSBs that require effective cell cycle checkpoint surveillance and coordinated repair (96). A hyper-sensitive and prolonged G2-M arrest, as observed here following reduced OFD1, could conceivably disrupt this delicate balance, impacting normal cortical development and thereby potentially contributing to the cortical abnormalities observed in OFD type I patients (neuronal migration/organisation disorders, pachygyria, gray matter heterotopias, cortical dysplasia, polymicrogyria and schizencephaly) (11). Our data show that the G2-M checkpoint abnormality we identified in OFD Type I patient cells is identical to

that observed following knockdown of *TIP60*. Again, this illustrates that impaired OFD1 can phenocopy loss of *TIP60* in certain circumstances.

In conclusion, we identify a series of novel and unanticipated cellular phenotypes associated with reduced OFD1 expression in OFD Type I patient cells. Our findings provide strong evidence that reduced OFD1 expression results in compromised DSB-induced histone modification, altered chromatin plasticity, defective HRR-mediated DSB repair and hypersensitive and prolonged cell cycle checkpoint arrest. Our results suggest that TIP60 mis-localization in OFD Type I likely underlie these phenotypes. Collectively, these observations provide functional contextualisation to the previously described interaction between OFD1 and the multisubunit TIP60 acetyltransferase complex. Furthermore, these findings extend our knowledge of the consequences of OFD1 dysfunction from its established roles at the centrosome/basal body/cilia network.

Materials and Methods.

Cell culture.

All cell lines were cultured at 37^{o}C in humidified incubators under 5% CO_2. LCLs were grown in RPMI1640 with 15% foetal calf serum, antibiotics (Pen-Strep) and L-Gln. Patient derived primary and hTERT-immortalised fibroblasts and control fibroblasts (1BR.3, MRC5VA) were grown in MEM with 15% foetal calf serum (FCS) supplemented with antibiotics (Pen-Strep) and L-Gln, whilst HeLa and HEK293 cells were grown in MEM with 10% FCS, Pen-Strep and L-Gln. U20S were cultured in McCoy's 5A supplemented with 10% FCS, Pen-Strep and L-Gln.

Antibodies.

The following antibodies were obtained from Cell Signalling Technology; H2A (#2578) and H2A-AcK5 (#2576). Antibodies obtained from Santa Cruz Technologies included: Lamin B (C-20. #sc-6216), RAD51 (H-92. #sc-8349) and TIP60 (N-17. #sc-5725) and CENP-F (H-260. #sc-22791). For IP of endogenous protein anti-TIP60 (#07-038) from EDM-Millipore was used and anti-TIP60 (H00010524-D01) from Abnova was also used for expression analysis. Anti- KAP1 (#A300-274A) and anti-53BP1 (#A300-272) were from Bethyl. The other antibodies used included those against α-tubulin (Sigma-Aldrich, #T5168), γH2AX (S139. Millipore, #05-636), PARP (AbDSerotec, #MCA1522), p85 PARP (Promega, #G734A), OFD1 (NovusBio, #NBP1-89356), H4 (Abcam, #ab10158) and H4-AcK16 (EMD-Millipore, #07-329).

Immunoprecipitation.

HEK293 cells were transfected with p3XFLAG-CMV10 expressing the human *OFD1* or with the empty vector. 48 hrs post-transfection, cells were lysed (10mM Tris HCl pH7.5,

NaCl 150mM, Triton 1%, supplemented with a cocktail of protease inhibitor (Sigma-Aldrich)) and total protein extracts pre-cleared twice with mouse IgG agarose beads (Sigma-Aldrich) at 4°C for 30min. Non-retained proteins were then incubated with M2 anti-FLAG agarose-conjugated antibody beads (Sigma-Aldrich) overnight at 4°C. The beads were then washed three times with the lysis buffer and the retained protein complexes eluted with 3XFLAG peptide, and loaded on polyacrylamide SDS-PAGE.

For IP of endogenous proteins from HeLa, cells were lysed in Buffer A (50mM Tris-HCl, 1mM EDTA, 10mM $MgCl_2$, 5mM EGTA, 0.5% Triton X-100 pH 7.3) and 500µg of total lysates were incubated for 1 hour with 5µg of specific antibodies or rabbit IgG as control, followed by for 1 hour of incubation with protein A-Sepharose beads. The unbound proteins were washed out twice with the Buffer A and once with the Buffer ST (50mM Tris-HCl, 150mM NaCl pH 7.3), while the bound fraction was analysed by western blot. Proteases Inhibitors from SIGMA (P8340) and PhosSTOP phosphatase inhibitors (both from Roche) were included throughout

Cellular Fractionation.

$5x10^7$ LCLs were extracted in 900µl of 0.1% NP40/PBS supplemented with complete protease inhibitors (Sigma-Aldrich). The supernatant (cytoplasmic fraction) was retained and nuclear pellet washed (PBS) and extracted with 100µl of 9M Urea/50mM Tris pH7.5 with β-mercaptoethanol and sonicated (20 sec at 30% amplitude using a microprobe) to solubilise the chromatin.

For chromatin extract preparation $1x10^7$ cells were washed in cold PBS, resuspended in 200 µL Hypotonic buffer (10 mM HEPES pH 7.5, 5mM KCl, 1.5 mM $MgCl_2$, 1mM DDT, 10 mM NaF, 1 mM Na_2VO_3, 10 mM β-glycerophosphate, 0.5% IGEPAL and Roche protease inhibitor cocktail) and incubated on ice for 15 min. The pelleted sample was washed twice in

200 µL of Hypotonic buffer and resuspended in 100 µL Hypotonic buffer containing 0.5 M NaCl and incubated for 15 min on ice. Chromatin was pelleted (17,000*xg* for 10 min), and solubilised in urea buffer (9M Urea, 50 mM Tris-HCl pH 7.5). Samples were sonicated for 10 sec at 30% Amplitude and resuspended in SDS buffer for loading on SDS-PAGE gels.

siRNA.

Cells were transfected using Metafectene Pro (Biontex; #T040-5.0) using ON-TARGETplus siRNA SmartPools (4x validated oligo mix per target). *OFD1* (#L-009300-00-0005) and *TIP60* (#L-006301-00-0005).

shOFD1 Lentiviral Transduction.

Lentiviral shRNA against *OFD1* were used as pre-made viral particles from Santa Cruz Technologies (#sc-91245-V) according to manufacturer's instructions on U2OS cells. Transduced clones were selected using 5µg/ml puromycin.

Immunofluorescence.

Fibroblasts grown on glass coverslips were washed in PBS, permeabilized for 30sec in 0.05% Triton/PBS, washed (PBS) and then fixed with 3% paraformaldehyde (PFA) with 2% sucrose for 10 min. Coverslips were then washed (PBS), blocked in 5% BSA/PBS for 30mins, prior to incubation with anti-TIP60 (Abcam; ab62644) for 1h. Following washing in PBS, coverslips were incubated with secondary anti goat-Cy3 (Sigma-Aldrich; #C2821) for 1h, counterstained with DAPI, and mounted in Vectashield (Vector Laboratories; #H-1000).

DSB repair analysis was assessed using IR-induced 53BP1 foci. Primary fibroblasts were grown to confluence for repair analysis in G0. For repair analysis in G2, cells were treated with 10µM aphidicolin following irradiation to prevent S-G2 transit, whilst 53BP1 foci were enumerated in G2 cells identified by strong staining with CENP-F.

Micrococcal nuclease chromatin digestion.

$5x10^6$ cells were used per digestion (1BR.3 and OFD:FB-2 or U2OS and U2OS shOFD1). Cells were either untreated (Unt) or treated with 2µg neocarzinostatin (Sigma; #N9162-100UG) for 30mins (Neo). To isolate nuclei cells were washed in PBS and resuspended in 300µl NIB buffer (15mM Tris HCl, pH 7.5; 25mM KCl; 10mM NaCl, 1mM $MgCl_2$; 1mM $CaCl_2$; 250mM Sucrose; 0.5mM DTT). Cells were subjected to two rounds of freeze/thaw using liquid nitrogen and pelleted by centrifugation at 4^0C for 10 mins. Supernatant was removed and the nuclear pellet resuspended in 350µl NIB buffer and treated with 3µl of MNase (Roche; #107921; 10U/µl) and digested at room temperature. 50µl samples were taken from the master digestion for each time point (2, 3, 4, 6, 8 and 10mins) and 50µl of stop buffer (2.4% SDS, 40mM EDTA, 20µg Proteinase K) added immediately and incubated at 37^0C for 10mins. Samples were then left on ice for DNA isolation. To each sample 50µl 1xTE buffer was added followed by 150µl of phenol:chloroform:isoamylalcohol (25:24:1). Following phase separation, 100µl of soluble fraction was transferred to a new tube and then mixed with 10µl 3M sodium acetate pH5.2, 750µl 100% ethanol and 1µl 10mg/ml glycogen (Sigma-Aldrich; #G8751). The resultant pellet was washed with 300µl 70% ethanol, dried and resuspended in 20µl 1xTE. 1µl of each sample was then run on Agilent 2100 Bioanalyser using Agilent DNA 12000 Kit (#5067-1508) and evaluated using the 2100 Expert DNA dsDNA 12000 laddering program.

G2-M checkpoint analysis.

For G2-M checkpoint activation analysis, LCLs were either untreated (Unt) or irradiated with increasing doses of IR (0.1, 0.2, 0.5Gy) before seeding into complete medium supplemented with 0.2mg/ml colcemid and incubated for 4hrs. LCLs were pelleted, swollen in 75mM KCL (10mins) and fixed in 3% PFA (10mins) prior to cytospinning onto poly-L-

lysine coated slides. Cells were counter-stained with DAPI and mounted in Vectashield prior to analysis on the Zeiss Axioplan platform. For the checkpoint recovery analysis, cells were allowed recover for 8hrs in the presence of a nocodazole trap (300nM).

HRR analysis using I-SceI GFP-assay.

DR-U2OS GFP cells were seeded at $2x10^5$ and subjected to transfection with the appropriate siRNA SmartPool system. 6hrs post-transfection cells were transfected with the appropriate vector systems (I-SceI expression vector, empty pCMV or GFP vector). Cells were incubated for 48hrs, harvested and run as live cell suspensions on the BD-Accuri FACS platform with data analysis via BD-CSampler Software.

Cell death and clonogenic survival.

Cell death analysis on LCLs was analysed 72hrs post IR (6 Gy) using the Dead Cell Apoptosis (Annexin V/Sytox Green) flow cytometry kit from ThermoFisher Scientific (V35113) according to the manufacturers' instructions. For clonogenic survival studies different numbers of cells (Ctrl: control vector. *OFD1* shRNA: lentiviral transduced with *OFD1* silencing shRNA) were seeded into 10-cm dishes with increasing concentrations of olaparib as indicated or following 4 Gy IR. After 14 days colonies were fixed in methanol and stained with methylene blue.

Funding.

This work was supported by a Cancer Research UK programme grant (C24110/A15394) to M.O'D and by the Italian Telethon Foundation (TMBFCB311TT) to B.F.

Conflict of interest statement.

The authors declare no conflict of interest.

Figure legends.

Figure 1.

OFD1 associates with TIP60 and OFD Type I patient cells exhibit mis-localization of TIP60.

(A). Interaction between OFD1 and TIP60 was demonstrated by co-immunoprecipitation (IP). HEK293 cells were transfected with p3XFlag-CMV10 containing *OFD1* (FLAG-*OFD1*) or empty vector (FLAG-Ev) and IP'd using M2 anti-FLAG agarose-conjugated antibody beads. Total lysate (TL) inputs and IPs were subsequently blotted for TIP60.

(B). Co-IP analysis of endogenous OFD1-TIP60 was performed on total lysates (TL) from Hela cells. IgG was used as loading control.

(C). Unperturbed exponentially growing 1BR.3 control wild-type (WT) fibroblasts exhibited pronounced nuclear staining for TIP60. This was in contrast to TIP60 staining pattern in two distinct OFD Type I patient fibroblast lines (OFD:FB-1 and OFD:FB-2). Both patient fibroblasts exhibited a more dispersed staining pattern with a preponderance of TIP60 appearing to localise to the cytoplasm, in contrast to WT fibroblasts. Scale bar: 20μm.

(D). The left-hand panel represents OFD1 expression analysis following siRNA mediated *OFD1* knockdown in 1BR.3 control wild-type (WT) fibroblasts (*OFD1* siRNA) compared to treatment with the control (Ctrl) scrambled siRNA. The right-hand immunofluorescence panels for these respective treatments show that following siRNA of *OFD1*, TIP60 localisation is dispersed from the nucleus; a similar staining pattern to that observed in the patient fibroblasts (C). Scale bar: 20μm.

Figure 2.

Nuclear TIP60 is reduced in OFD Type I patient cells.

(A). Wild-type (WT) and OFD Type 1 patient fibroblasts (OFD: FB-2) were subjected to sub-cellular fractionation and the cytoplasmic (Cyto) and nuclear (Nuc) fractions analysed alongside WCE (Total) for TIP60 expression. Lamin B served as a quality control indicator for nuclear fraction purity whilst α-tubulin served a similar purpose for the cytoplasmic extract. The nuclear fraction derived from the OFD Type I patient fibroblasts contained less TIP60 compared to that of the WT LCLs (bottom right-hand panel).

(B). 25μg and 50μg of whole cell extract (WCE) from wild-type (WT) and OFD Type I patient LCLs were probed for OFD1 expression by western blotting. OFD1 was markedly reduced in OFD Type I LCLs.

(C). OFD1 was detectable in a chromatin extract from wild-type (WT) LCLs in contrast to OFD Type I LCLs (OFD Type I). Blotting for the facultative heterochromatin protein KAP1 was used as a loading control.

(D). Sub-cellular fraction analysis was also performed on wild-type (WT) and OFD Type 1 fibroblasts (OFD: FB-2). Reduced level of TIP60 was observed in the nuclear fraction of the OFD Type I patient cells (bottom panel, right-hand side).

(E). Differing amounts of high-salt chromatin extracts (8, 4, 2μg) prepared from wild-type (WT) and OFD Type I patient LCLs were probed for TIP60 levels by western blotting. Blotting for the facultative heterochromatin protein KAP1 was used as a loading control. The right-hand plot represents a quantitation of TIP60 levels (a.u. arbitrary units) using ImageJ software. Data represents the mean + S.D. (n=3) (* $P<0.05$ Student's *t*-test). OFD Type I patient LCLs exhibit reduced TIP60 on chromatin compared to wild-type (WT) LCLs.

(F). The left-hand panel shows OFD1 expression analysis by western blot of U2OS cells stably transduced with lentiviral shRNA directed against *OFD1* (*OFD1* shRNA) compared to cells transduced with control (Ctrl) shRNA vector. In the right-hand panel differing amounts of high-salt chromatin extracts (20, 10, 5μg) prepared from these cells were probed for TIP60 levels by western blotting. Blotting for the facultative heterochromatin protein KAP1 was used as a loading control. *OFD1* shRNA in U2OS exhibit reduced TIP60 on chromatin compared to control (Ctrl) shRNA.

Figure 3.

OFD Type I patient cells exhibit reduced IR-induced histone modification, including acetylation of H2A and H4, consistent with impaired TIP60 HAT activity.

(A). Upper panel depicts the IR-induced (10Gy) acetylation of histone H2A on lysine-5 (H2A-AcK5) at different times post irradiation (0, 5, 15, 30mins post-IR) in wild-type (WT) fibroblasts and OFD Type I patient derived fibroblasts (OFD:FB-2). The same samples were subjected to western blotting using anti-γH2AX (short and long exposure). In the long exposure, the slower migrating modified form of γH2AX (*Mod*-γH2AX) is enriched in the WT extracts following IR, in contrast to those of the OFD Type I cells. This species is consistent with post-translationally modified (monoubiquitinated, phosphorylated, acetylated) form of H2AX. Attenuated IR-induced H2A-AcK5 and slower migrating γH2AX (*Mod*-γH2AX) are seen in the OFD Type I patient fibroblast compared to WT.

(B). Control 1BR.3 wild-type (WT) fibroblasts were subjected to siRNA using control (Ctrl) scrambled oligos and siRNA SmartPools against *OFD1* and *TIP60*. 48hrs post transfection cells were irradiated (10Gy) and incubated for increasing times (0, 5, 15, 30mins post-IR) before western blotting for H2A-AcK5 and γH2AX. Increased IR-induced H2A-AcK5 was

observed in Ctrl cells in contrast to those subjected to either *OFD1* or *TIP60* siRNA. Similar to (A), IR-induced *Mod*-γH2AX formation was reduced following *OFD1*, and also following *TIP60* siRNA compared to Ctrl.

(C). Control wild-type (WT) and OFD Type I patient fibroblasts (OFD:FB-2) were irradiated (10Gy) and acetylation of histone H4 on lysine-16 (H4-AcK16) was assessed at different times post-irradiation (0, 5, 15, 30mins post-IR). An increase in H4-AcK16 formation was observed in WT cells up to 15mins post-IR, followed by a steep decline at 30mins. In contrast, H4-AcK16 levels did not increase after IR in OFD Type I patient fibroblasts, rather remaining static up to 15mins.

(D). U2OS cells were subjected to siRNA using control (Ctrl) scrambled oligos and siRNA SmartPools against *OFD1* and *TIP60*. 48hrs post transfection cells were irradiated (10Gy) and incubated for increasing times (0, 5, 15, 30mins) before western blotting for H4-AcK16. A time dependent increase in IR-induced H4-AcK16 was observed in Ctrl cells in contrast to those subjected to *OFD1* siRNA, which responded similarly to the patient-derived fibroblasts (C). *TIP60* siRNA (bottom panel, left-hand side) strongly reduced IR-induced H4-AcK16 (lower panel right-hand side) attesting to the TIP60-dependent nature of this histone acetylation.

Figure 4.

OFD Type I patient cells exhibit reduced micrococcal nuclease chromatin digestion following DSBs.

(A). Nuclei isolated from wild-type (WT) and OFD Type I patient fibroblasts (OFD: FB-2) were subjected to micrococcal nuclease (MNase) digestion to evaluate chromatin dynamics.

The appearance of fully digested chromatin down to mononucleosome-sized DNA fragments was monitored using the Agilent 2100 Bioanalyser and DNA chips, with the digestion profiles generated using the 2100 Expert DNA dsDNA 12000 laddering software. A typical digestion profile from untreated fibroblasts (Unt) is shown in the left-hand side with mononucleosome-sized DNA fragments and various polynucleosome species indicated (Mono-, Di-, Tri). No significant change in profiles was observed between WT fibroblasts and OFD Type I patient fibroblasts following digestion up to 10mins under these conditions. In contrast, digestion profiles generated from cells treated with the radiomimetic neocarzinostatin (Neo) did show differences in digestion profiles. The right-hand panel shows a profile generated following 6mins digestion with MNase, clearly demonstrating the reduced level of digestion products (mononucleosomes and polynucleosomes) detected from the OFD Type I patient cells.

(B). The rate of generation of mononucleosome species was determined over time as indicated, normalised to mononucleosome levels following 2mins MNase digestion. A statistically significant difference (* $P<0.05$ Student's *t*-test) in MNase accessibility is observed from 6mins (*NS; not significant*) wherein the OFD Type I patient fibroblasts demonstrate a reduction in MNase accessible chromatin following treatment with neocarzinostatin. Data represents the mean $\pm$ S.D. of five separate digestion profiles.

(C). OFD1 expression is markedly reduced in U2OS cells stably transduced with lentiviral shRNA directed against *OFD1* (*OFD1* shRNA) compared to cells transduced with control (Ctrl) shRNA vector.

(D). Similar to the OFD Type I patient fibroblasts (B), MNase accessibility following neocarzinostatin treatment is reduced in *OFD1* shRNA cells compared to control (Ctrl) from 6mins digestion with MNase (* $P<0.05$ Student's *t*-test. *NS; not significant*). Data represents the mean $\pm$ S.D. of four independent determinations.

Figure 5.

OFD Type I patient cells exhibit impaired Homologous Recombination Repair (HRR) of DSBs.

(A). Control wild-type (WT) and OFD Type I patient primary fibroblasts (OFD: FB.1 and OFD: FB.2) were grown to confluency and DSB repair in G0 cells was determined following 3Gy IR at the times indicated by IF staining and enumeration of 53BP1 foci. The rate of disappeared of IR-induced 53BP1 foci under these conditions (NHEJ) is comparable WT and OFD Type I fibroblasts.

(B). DSB repair in G2 cells, identified by CENP-F staining was similarly assessed using 53BP1 foci 7.5 hrs post IR. OFD Type I fibroblasts (OFD: FB.1) exhibit elevated levels of IR-induced 53BP1 foci/G2 cell compared to control wild-type (WT) consistent with impaired DSB repair in G2. Data represents the mean $\pm$ S.D. of three independent experiments (*P<0.05 Student's t-test)

(C). Control wild-type (WT) and OFD Type I patient fibroblasts (OFD: FB.2) were monitored for DSB-induced RAD51 formation by indirect immunofluorescence (IF) staining for cells containing RAD51 foci. Cells were either untreated (Unt) or irradiated with 2Gy (IR) and foci positive cells enumerated at 4hrs post-IR. OFD Type I fibroblasts exhibited a >50% reduction in RAD51 positive cells compared to WT fibroblasts under these conditions. Data represents the mean $\pm$ S.D. of four independent determinations (* P<0.05 Student's t-test).

(D). DSB-induced RAD51 foci formation was also assessed by IF in U2OS cells transduced with control shRNA (Ctrl) and shRNA targeting *OFD1* (*OFD1* shRNA). Cells were either untreated (Unt) or irradiated with 2Gy (IR) and foci positive cells enumerated 4hrs post-IR. Knockdown of *OFD1* significantly (* P<0.05 Student's t-test) reduced RAD51 foci

formation under these conditions. Data represents the mean ± S.D. of four independent determinations.

(E). The efficacy of I-SceI mediated HRR was evaluated using an integrated DR-GFP system in U2OS cells following siRNA knockdown of either *OFD1* or *TIP60*. Silencing of either *OFD1* or *TIP60* resulted in a significant reduction in HRR of an I-SceI-induced DSB (*P<0.05 Student's *t*-test). Data represents the mean ± S.D. of four independent experiments.

Figure 6.

(A). Wild-type (WT) and OFD Type I patient LCLs irradiated with 6Gy IR and % cell death determined 72hrs post-IR using flow cytometry-based Annexin V/Sytox Green analysis. OFD Type I LCLs exhibited elevated cell death compared to control wild-type (WT) LCLs under these conditions. Data represents the mean ± S.D. of three independent experiments (*P<0.05 Student's *t*-test).

(B). Clonogenic survival analysis of U20S transduced with control vector (Ctrl) or lentiviral shRNA towards *OFD1* (*OFD1* shRNA) following 4Gy IR. Surviving colonies were scored 14 days following plating. *OFD1* shRNA in U2OS was associated with reduced clonal survival compared to control (Ctrl) shRNA under these conditions. Data represents the mean ± S.D. of three independent experiments (* P<0.05 Student's *t*-test).

(C). Wild-type (WT) and OFD Type I patient LCLs were treated with increasing concentrations of olaparib (0, 50, 100, 150μM) for 48hrs. Apoptosis was detected by western blotting for the presence of the p85KD caspase-cleaved form of PARP. Elevated levels of p85-PARP were detectable at all concentrations of olaparib following treatment of the OFD Type I LCLs compared to WT LCLs.

(D). Clonogenic survival analysis of U20S transduced with control vector (Ctrl) or lentiviral shRNA towards *OFD1* (*OFD1* shRNA) following treatment with different concentrations of olaparib. Surviving colonies were scored 14 days following plating. Consistent with the compromised HRR observed following siRNA of OFD1 and the elevated olaparib-induced apoptosis seen in OFD Type I patient LCLs, *OFD1* shRNA specifically exhibited elevated sensitivity to killing by olaparib.

Figure 7.

OFD Type I patient cells exhibit a hypersensitive DSB-induced G2-M checkpoint arrest and delayed recovery.

(A). LCLs from normal wild-type (WT) and OFD Type I individuals were irradiated with increasing doses of IR and the mitotic index determined in the presence of colcemid at 4hrs post-IR. OFD Type I LCLs demonstrated a robust G2 arrest at doses as low as 0.1Gy, in contrast to WT LCLs (* $P<0.05$ Student's *t*-test). Data represents the mean $\pm$ S.D. of four independent determinations. These results indicate that OFD Type I LCLs exhibit hypersensitive activation of the DSB-induced G2-M cell cycle checkpoint.

(B). Recovery from G2-M checkpoint activation and arrest following 1Gy IR was monitored in wild-type (WT) and OFD Type I LCLs. At 8hrs post-IR in the presence of a nocodazole trap, only approximately 30% recovery (i.e. progression from G2 into M phase) was observed in OFD Type I LCLs compared to circa 75% recovery of WT LCLs. These results indicate that OFD Type I LCLs exhibit impaired recovery from activation of the DSB-induced G2-M cell cycle checkpoint compared to WT LCLs. Error bars represent the mean $\pm$ S.D. of four independent experiments (* $P<0.05$ Student's *t*-test).

(C). MRC5VA fibroblasts were subjected to siRNA using control (Ctrl) scrambled oligos and siRNA SmartPools against *OFD1* and *TIP60*. 48hrs post transfection cells were irradiated with 2Gy IR and mitotic recovery determined 8hrs post IR in the presence of a nocodazole trap. At this time Ctrl cells showed around a 70% recovery in contrast to approximate 30% recovery seen following siRNA of either *OFD1* or *TIP60*. Similar to OFD Type I LCLs, siRNA knockdown of *OFD1* results in impaired recovery from DSB-induced G2-M cell cycle checkpoint activation. This impaired recovery is also seen following siRNA of *TIP60*. Error bars represent the mean $\pm$ S.D. of four independent experiments (* $P<0.05$ Student's *t*-test).

Supplementary Figure 1.

OFD Type I patient cells exhibit attenuated ionising radiation (IR)-induced ATM signalling.

(A). Control wild-type (WT) and OFD Type I patient LCLs were irradiated (3Gy IR) and cells incubated for different times (0, 5, 15, 30mins post-IR) prior to extraction and analysis for ATM autophosphorylation on serine 1981 and ATM-dependent phosphorylation of NBS1, MRE11, KAP1 and CHK2, as indicated. With the exception of ATM autophosphorylation where the effect was more muted, attenuated DSB-induced phosphorylation appears a feature of the OFD Type I patient LCLs compared to those of WT, indicating sub-optimal ATM activation under these conditions.

(B). A549 cells were transfected with control scrambled oligos (Ctrl) or a SmartPool directed against *OFD1*. 48hrs post-transfection cells were irradiated (3Gy IR) and extracts prepared at differing times post-irradiation (0, 5, 15, 30mins post-IR). Levels of phosphorylated ATM,

NBS1, KAP1 and CHK2 were then assessed following western blotting. siRNA silencing of *OFD1* impaired IR-induced phosphorylation of these targets.

References

1 Gurrieri, F., Franco, B., Toriello, H. and Neri, G. (2007) Oral -facial-digital syndromes: a review and diagnostic guidelines. *Am J Med Genet*, 143A, 3314 - 3323.

2 Macca, M. and Franco, B. (2009) The molecular basis of oral-facial-digital syndrome, type 1. *American Journal of Medical Genetics Part C: Seminars in Medical Genetics*, 151C, 318-325.

3 Franco, B. and Thauvin-Robinet, C. (2016) Update on oral-facial-digital syndromes (OFDS). *Cilia*, 5, 1-11.

4 Ferrante, M., Giorgio, G., Feather, S., Bulfone, A., Wright, V., Ghiani, M., Selicorni, A., Gammaro, L., Scolari, F., Woolf, A. *et al.* (2001) Identification of the gene for oral-facial-digital type I syndrome. *Am J Hum Genet*, 68, 569 - 576.

5 de Conciliis, L., Marchitiello, A., Wapenaar, M., Borsani, G., Giglio, S., Mariani, M., Consalez, G., Zuffardi, O., Franco, B., Ballabio, A. *et al.* (1998) Characterization of Cxorf5 (71-7A), a novel human cDNA mapping to Xp22 and encoding a protein containing coiled-coil a-helical domains. *Genomics*, 51, 243 - 250.

6 Thauvin-Robinet, C., Thomas, S., Sinico, M., Aral, B., Burglen, L., Gigot, N., Dollfus, H., Rossignol, S., Raynaud, M., Philippe, C. *et al.* (2013) OFD1 mutations in males: phenotypic spectrum and ciliary basal body docking impairment. *Clin Genet*, 84, 86 - 90.

7 Prattichizzo, C., Macca, M., Novelli, V., Giorgio, G., Barra, A. and Franco, B. (2008) Mutational spectrum of the oral-facial-digital type I syndrome: a study on a large collection of patients. *Hum Mutat*, 29, 1237 - 1246.

8 Thauvin-Robinet, C., Franco, B., Saugier-Veber, P., Aral, B., Gigot, N., Donzel, A., Van Maldergem, L., Bieth, E., Layet, V., Mathieu, M. *et al.* (2009) Genomic deletions

of OFD1 account for 23% of oral-facial-digital type 1 syndrome after negative DNA sequencing. *Hum Mutat*, 30, E320 - E329.

9 Bisschoff, I., Zeschnigk, C., Horn, D., Wellek, B., Riess, A., Wessels, M., Willems, P., Jensen, P., Busche, A., Bekkebraten, J. *et al.* (2013) Novel mutations including deletions of the entire OFD1 gene in 30 families with type 1 orofaciodigital syndrome: a study of the extensive clinical variability. *Hum Mutat*, 34, 237 - 247.

10 Toriello, H.V., Franco, B., Bruel, A.L. and Thauvin-Robinet, C. (2002) *Oral-Facial-Digital Syndrome Type I.* University of Washington, Seattle, Seattle (WA).

11 Del Giudice, E., Macca, M., Imperati, F., D'Amico, A., Parent, P., Pasquier, L., Layet, V., Lyonnet, S., Stamboul-Darmency, V., Thauvin-Robinet, C. *et al.* (2014) CNS involvement in OFD1 syndrome: a clinical, molecular, and neuroimaging study. *Orphanet Journal of Rare Diseases*, 9, 74.

12 Gerlitz, G., Darhin, E., Giorgio, G., Franco, B. and Reiner, O. (2005) Novel Functional Features of the LIS-H Domain: Role in Protein Dimerization, Half-Life and Cellular Localization. *Cell Cycle*, 4, 1632-1640.

13 Burkhard, P., Stetefeld, J. and Strelkov, S.V. (2001) Coiled coils: a highly versatile protein folding motif. *Trends in Cell Biology*, 11, 82-88.

14 Ferrante, M., Zullo, A., Barra, A., Bimonte, S., Messaddeq, N., Studer, M., Dolle, P. and Franco, B. (2006) Oral-facial-digital type I protein is required for primary cilia formation and left-right axis specification. *Nat Genet*, 38, 112 - 117.

15 Bimonte, S., De Angelis, A., Quagliata, L., Giusti, F., Tammaro, R., Dallai, R., Ascenzi, M.-G., Diez-Roux, G. and Franco, B. (2011) Ofd1 is required in limb bud patterning and endochondral bone development. *Developmental Biology*, 349, 179-191.

16 D'Angelo, A., De Angelis, A., Avallone, B., Piscopo, I., Tammaro, R., Studer, M. and Franco, B. (2012) Ofd1 controls Dorso-Ventral patterning and axoneme elongation during embryonic brain development. *PLoS ONE*, 7, e52937.

17 Ferrante, M.I., Romio, L., Castro, S., Collins, J.E., Goulding, D.A., Stemple, D.L., Woolf, A.S. and Wilson, S.W. (2009) Convergent extension movements and ciliary function are mediated by ofd1, a zebrafish orthologue of the human oral-facial-digital type 1 syndrome gene. *Human Molecular Genetics*, 18, 289-303.

18 Romio, L., Wright, V., Price, K., Winyard, P., Donnai, D., Porteous, M., Franco, B., Giorgio, G., Malcolm, S., Woolf, A. *et al.* (2003) OFD1, the gene mutated in Oral-Facial-Digital Syndrome Type 1, is expressed in the metanephros and in human embryonic renal mesenchymal cells. *J Am Soc Nephrol*, 14, 680 - 689.

19 Giorgio, G., Alfieri, M., Prattichizzo, C., Zullo, A., Cairo, S. and Franco, B. (2007) Functional characterization of the OFD1 protein reveals a nuclear localization and physical interaction with subunits of a chromatin remodeling complex. *Mol Biol Cell*, 18, 4397 - 4404.

20 Lopes, C.A.M., Prosser, S.L., Romio, L., Hirst, R.A., O'Callaghan, C., Woolf, A.S. and Fry, A.M. (2011) Centriolar satellites are assembly points for proteins implicated in human ciliopathies, including oral-facial-digital syndrome 1. *J. Cell Science*, 124, 600-612.

21 Singla, V., Romaguera-Ros, M., Garcia-Verdugo, J. and Reiter, J. (2010) Ofd1, a human disease gene, regulates the length and distal structure of centrioles. *Dev Cell*, 18, 410 - 424.

22 Tang, Z., Lin, M.G., Stowe, T.R., Chen, S., Zhu, M., Stearns, T., Franco, B. and Zhong, Q. (2013) Autophagy promotes primary ciliogenesis by removing OFD1 from centriolar satellites. *Nature*, 502, 254-257.

23 Pampliega, O., Orhon, I., Patel, B., Sridhar, S., Diaz-Carretero, A., Beau, I., Codogno, P., Satir, B.H., Satir, P. and Cuervo, A.M. (2013) Functional interaction between autophagy and ciliogenesis. *Nature*, 502, 194-200.

24 Yangfan P. Liu, I-Chun Tsai, Manuela Morleo, Edwin C. Oh, Carmen C. Leitch, Filomena Massa, Byung-Hoon Lee, David S. Parker, Daniel Finley, Norann A. Zaghloul *et al.* (2014) Ciliopathy proteins regulate paracrine signaling by modulating proteasomal degradation of mediators. *J Clin Invest*, 124, 2059-2070.

25 Carrozza, M.J., Utley, R.T., Workman, J.L. and Côté, J. (2003) The diverse functions of histone acetyltransferase complexes. *Trends in Genetics*, 19, 321-329.

26 Sun, Y., Jiang, X., Chen, S., Fernandes, N. and Price, B.D. (2005) A role for the Tip60 histone acetyltransferase in the acetylation and activation of ATM. *Proc. Nat. Acad. Sci. USA*, 102, 13182-13187.

27 Sun, Y., Xu, Y., Roy, K. and Price, B.D. (2007) DNA Damage-Induced Acetylation of Lysine 3016 of ATM Activates ATM Kinase Activity. *Molecular and Cellular Biology*, 27, 8502-8509.

28 Sun, Y., Jiang, X., Xu, Y., Ayrapetov, M.K., Moreau, L.A., Whetstine, J.R. and Price, B.D. (2009) Histone H3 methylation links DNA damage detection to activation of the tumour suppressor Tip60. *Nat Cell Biol*, 11, 1376-1382.

29 Murr, R., Loizou, J.I., Yang, Y.-G., Cuenin, C., Li, H., Wang, Z.-Q. and Herceg, Z. (2006) Histone acetylation by Trrap-Tip60 modulates loading of repair proteins and repair of DNA double-strand breaks. *Nat Cell Biol*, 8, 91-99.

30 Tang, J., Cho, N.W., Cui, G., Manion, E.M., Shanbhag, N.M., Botuyan, M.V., Mer, G. and Greenberg, R.A. (2013) Acetylation limits 53BP1 association with damaged chromatin to promote homologous recombination. *Nat Struct Mol Biol*, 20, 317-325.

31 Squatrito, M., Gorrini, C. and Amati, B. (2006) Tip60 in DNA damage response and growth control: many tricks in one HAT. *Trends in Cell Biology*, 16, 433-442.

32 Sun, Y., Jiang, X. and Price, B.D. (2010) Tip60: Connecting chromatin to DNA damage signaling. *Cell Cycle*, 9, 930-936.

33 Downs, J.A., Allard, S., Jobin-Robitaille, O., Javaheri, A., Auger, A., Bouchard, N., Kron, S.J., Jackson, S.P. and Côté, J. (2004) Binding of Chromatin-Modifying Activities to Phosphorylated Histone H2A at DNA Damage Sites. *Molecular Cell*, 16, 979-990.

34 Jha, S. and Dutta, A. (2009) RVB1/RVB2: Running Rings around Molecular Biology. *Molecular Cell*, 34, 521-533.

35 Jha, S., Gupta, A., Dar, A. and Dutta, A. (2013) RVBs Are Required for Assembling a Functional TIP60 Complex. *Molecular and Cellular Biology*, 33, 1164-1174.

36 Thauvin-Robinet, C., Cossée, M., Cormier-Daire, V., Van Maldergem, L., Toutain, A., Alembik, Y., Bieth, E., Layet, V., Parent, P., David, A. *et al.* (2006) Clinical, molecular, and genotype–phenotype correlation studies from 25 cases of oral–facial–digital syndrome type 1: a French and Belgian collaborative study. *J. Med. Genet.*, 43, 54-61.

37 Panier, S. and Durocher, D. (2013) Push back to respond better: regulatory inhibition of the DNA double-strand break response. *Nat Rev Mol Cell Biol*, 14, 661-672.

38 Fischle, W. (2009) Tip60-ing the balance in DSB repair. *Nat Cell Biol*, 11, 1279-1281.

39 Ikura, T., Tashiro, S., Kakino, A., Shima, H., Jacob, N., Amunugama, R., Yoder, K., Izumi, S., Kuraoka, I., Tanaka, K. *et al.* (2007) DNA Damage-Dependent Acetylation and Ubiquitination of H2AX Enhances Chromatin Dynamics. *Mol. Cell. Biol.*, 27, 7028-7040.

40 Ikura, T., Tashiro, S., Kakino, A., Shima, H., Jacob, N., Amunugama, R., Yoder, K., Izumi, S., Kuraoka, I., Tanaka, K. *et al.* (2007) DNA Damage-Dependent Acetylation and Ubiquitination of H2AX Enhances Chromatin Dynamics. *Molecular and Cellular Biology*, 27, 7028-7040.

41 Kimura, A. and Horikoshi, M. (1998) Tip60 acetylates six lysines of a specific class in core histones in vitro. *Genes to Cells*, 3, 789-800.

42 Stiff, T., O'Driscoll, M., Rief, N., Iwabuchi, K., Lobrich, M. and Jeggo, P.A. (2004) ATM and DNA-PK function redundantly to phosphorylate H2AX following exposure to ioninsing radiation. *Cancer Res.*, 64, 2390-2396.

43 Suka, N., Luo, K. and Grunstein, M. (2002) Sir2p and Sas2p opposingly regulate acetylation of yeast histone H4 lysine16 and spreading of heterochromatin. *Nat Genet*, 32, 378-383.

44 Kimura, A., Umehara, T. and Horikoshi, M. (2002) Chromosomal gradient of histone acetylation established by Sas2p and Sir2p functions as a shield against gene silencing. *Nat Genet*, 32, 370-377.

45 Yang, X.J. (2004) The diverse superfamily of lysine acetyltransferases and their roles in leukemia and other diseases. *Nucleic Acids Res.*, 32, 959-976.

46 Sharma, G.G., So, S., Gupta, A., Kumar, R., Cayrou, C., Avvakumov, N., Bhadra, U., Pandita, R.K., Porteus, M.H., Chen, D.J. *et al.* (2010) MOF and Histone H4 Acetylation at Lysine 16 Are Critical for DNA Damage Response and Double-Strand Break Repair. *Molecular and Cellular Biology*, 30, 3582-3595.

47 Li, X., Corsa, C.A.S., Pan, P.W., Wu, L., Ferguson, D., Yu, X., Min, J. and Dou, Y. (2010) MOF and H4 K16 Acetylation Play Important Roles in DNA Damage Repair by Modulating Recruitment of DNA Damage Repair Protein Mdc1. *Molecular and Cellular Biology*, 30, 5335-5347.

48 Gupta, A., Hunt, Clayton R., Hegde, Muralidhar L., Chakraborty, S., Udayakumar, D., Horikoshi, N., Singh, M., Ramnarain, Deepti B., Hittelman, Walter N., Namjoshi, S. *et al.* (2014) MOF Phosphorylation by ATM Regulates 53BP1-Mediated Double-Strand Break Repair Pathway Choice. *Cell Reports*, 8, 177-189.

49 Goodarzi, A.A., Noon, A.T., Deckbar, D., Ziv, Y., Shiloh, Y., Löbrich, M. and Jeggo, P.A. (2008) ATM Signaling Facilitates Repair of DNA Double-Strand Breaks Associated with Heterochromatin. *Molecular Cell*, 31, 167-177.

50 Noon, A.T., Shibata, A., Rief, N., Lobrich, M., Stewart, G.S., Jeggo, P.A. and Goodarzi, A.A. (2010) 53BP1-dependent robust localized KAP-1 phosphorylation is essential for heterochromatic DNA double-strand break repair. *Nat Cell Biol*, 12, 177-184.

51 Xu, Y., Ayrapetov, Marina K., Xu, C., Gursoy-Yuzugullu, O., Hu, Y. and Price, Brendan D. (2012) Histone H2A.Z Controls a Critical Chromatin Remodeling Step Required for DNA Double-Strand Break Repair. *Molecular Cell*, 48, 723-733.

52 Gursoy-Yuzugullu, O., Ayrapetov, M.K. and Price, B.D. (2015) Histone chaperone Anp32e removes H2A.Z from DNA double-strand breaks and promotes nucleosome reorganization and DNA repair. *Proceedings of the National Academy of Sciences*, 112, 7507-7512.

53 Hanan E Alatwi, J.A.D. (2015) Removal of H2A.Z by INO80 promotes homologous recombination. *EMBO Rep*, 16, 986-994.

54 Shogren-Knaak, M., Ishii, H., Sun, J.-M., Pazin, M.J., Davie, J.R. and Peterson, C.L. (2006) Histone H4-K16 Acetylation Controls Chromatin Structure and Protein Interactions. *Science*, 311, 844-847.

55 Ziv, Y., Bielopolski, D., Galanty, Y., Lukas, C., Taya, Y., Schultz, D.C., Lukas, J., Bekker-Jensen, S., Bartek, J. and Shiloh, Y. (2006) Chromatin relaxation in response to

DNA double-strand breaks is modulated by a novel ATM- and KAP-1 dependent pathway. *Nat Cell Biol*, 8, 870-876.

56 Xu, Y., Sun, Y., Jiang, X., Ayrapetov, M.K., Moskwa, P., Yang, S., Weinstock, D.M. and Price, B.D. (2010) The p400 ATPase regulates nucleosome stability and chromatin ubiquitination during DNA repair. *The Journal of Cell Biology*, 191, 31-43.

57 Cao, L., Xu, X., Bunting, S.F., Liu, J., Wang, R.-H., Cao, L.L., Wu, J.J., Peng, T.-N., Chen, J., Nussenzweig, A. *et al.* (2009) A Selective Requirement for 53BP1 in the Biological Response to Genomic Instability Induced by Brca1 Deficiency. *Molecular Cell*, 35, 534-541.

58 Bunting, S.F., Callén, E., Wong, N., Chen, H.-T., Polato, F., Gunn, A., Bothmer, A., Feldhahn, N., Fernandez-Capetillo, O., Cao, L. *et al.* (2010) 53BP1 Inhibits Homologous Recombination in Brca1-Deficient Cells by Blocking Resection of DNA Breaks. *Cell*, 141, 243-254.

59 Bouwman, P., Aly, A., Escandell, J.M., Pieterse, M., Bartkova, J., van der Gulden, H., Hiddingh, S., Thanasoula, M., Kulkarni, A., Yang, Q. *et al.* (2010) 53BP1 loss rescues BRCA1 deficiency and is associated with triple-negative and BRCA-mutated breast cancers. *Nat Struct Mol Biol*, 17, 688-695.

60 Chapman, J.R., Sossick, A.J., Boulton, S.J. and Jackson, S.P. (2012) BRCA1-associated exclusion of 53BP1 from DNA damage sites underlies temporal control of DNA repair. *J. Cell Science*, 125, 3529-3534.

61 Chapman, J.R., Taylor, Martin R.G. and Boulton, Simon J. (2012) Playing the End Game: DNA Double-Strand Break Repair Pathway Choice. *Molecular Cell*, 47, 497-510.

62 Bryant, H.E., Schultz, N., Thomas, H.D., Parker, K.M., Flower, D., Lopez, E., Kyle, S., Meuth, M., Curtin, N.J. and Helleday, T. (2005) Specific killing of BRCA2-deficient tumours with inhibitors of poly(ADP-ribose) polymerase. *Nature*, 434, 913-917.

63 Farmer, H., McCabe, N., Lord, C.J., Tutt, A.N.J., Johnson, D.A., Richardson, T.B., Santarosa, M., Dillon, K.J., Hickson, I., Knights, C. *et al.* (2005) Targeting the DNA repair defect in BRCA mutant cells as a therapeutic strategy. *Nature*, 434, 917-921.

64 Helleday, T. (2010) Homologous recombination in cancer development, treatment and development of drug resistance. *Carcinogenesis*, 31, 955960.

65 Toriello, H.V. and Franco, B. (1993) Pagon, R.A., Adam, M.P., Ardinger, H.H., Wallace, S.E., Amemiya, A., Bean, L.J.H., Bird, T.D., Fong, C.T., Mefford, H.C., Smith, R.J.H. and Stephens, K. (eds.), In *GeneReviews(R)*. University of Washington, Seattle, Seattle WA.

66 Zullo, A., Iaconis, D., Barra, A., Cantone, A., Messaddeq, N., Capasso, G., Dollé, P., Igarashi, P. and Franco, B. (2010) Kidney-specific inactivation of Ofd1 leads to renal cystic disease associated with upregulation of the mTOR pathway. *Human Molecular Genetics*, 19, 2792-2803.

67 Johnson, C.A. and Collis, S.J. (2016) Ciliogenesis and the DNA damage response: a stressful relationship. *Cilia*, 5, 1-13.

68 Bicknell, L.S., Bongers, E.M.H.F., Leitch, A., Brown, S., Schoots, J., Harley, M.E., Aftimos, S., Al-Aama, J.Y., Bober, M., Brown, P.A.J. *et al.* (2011) Mutations in the pre-replication complex cause Meier-Gorlin syndrome. *Nat Genet*, 43, 356-359.

69 Bicknell, L.S., Walker, S., Klingseisen, A., Stiff, T., Leitch, A., Kerzendorfer, C., Martin, C.-A., Yeyati, P., Al Sanna, N., Bober, M. *et al.* (2011) Mutations in ORC1, encoding the largest subunit of the origin recognition complex, cause microcephalic primordial dwarfism resembling Meier-Gorlin syndrome. *Nat Genet*, 43, 350-355.

70 Guernsey, D.L., Matsuoka, M., Jiang, H., Evans, S., Macgillivray, C., Nightingale, M., Perry, S., Ferguson, M., LeBlanc, M., Paquette, J. *et al.* (2011) Mutations in origin recognition complex gene ORC4 cause Meier-Gorlin syndrome. *Nat Genet*, 43, 360-364.

71 Stiff, T., Alagoz, M., Alcantara, A., Outwin, E., Brunner, H.G., Bongers, E.M.H.F., O'Driscoll, M. and Jeggo, P.A. (2013) Deficiency in Origin Licensing proteins impairs cilia formation: implications for the aetiology of Meier-Gorlin syndrome. *PLoS Genet*, 9, e1003360.

72 O'Driscoll, M., Ruiz-Perez, V.L., Woods, C.G., Jeggo, P.A. and Goodship, J.A. (2003) A splicing mutation affecting expression of ataxia-telangiectasia and Rad3-related protein (ATR) results in Seckel syndrome. *Nature Genetics*, 33, 497-501.

73 Ogi, T., Walker, S., Stiff, T., Hobson, E., Limsirichaikul, S., Carpenter, G., Prescott, K., Suri, M., Byrd, P.J., Matsuse, M. *et al.* (2012) Identification of the First ATRIP–Deficient Patient and Novel Mutations in ATR Define a Clinical Spectrum for ATR–ATRIP Seckel Syndrome. *PLoS Genet*, 8, e1002945.

74 Valdés-Sánchez, L., De la Cerda, B., Diaz-Corrales, F.J., Massalini, S., Chakarova, C.F., Wright, A.F. and Bhattacharya, S.S. (2013) ATR localizes to the photoreceptor connecting cilium and deficiency leads to severe photoreceptor degeneration in mice. *Human Molecular Genetics*, 22, 1507-1515.

75 Stiff, T., Casar Tena, T., O'Driscoll, M., Jeggo, P.A. and Philipp, M. (2016) ATR promotes cilia signalling: links to developmental impacts. *Human Molecular Genetics*, 25, 1574-1587.

76 Chaki, M., Airik, R., Ghosh, Amiya K., Giles, Rachel H., Chen, R., Slaats, Gisela G., Wang, H., Hurd, Toby W., Zhou, W., Cluckey, A. *et al.* (2012) Exome

Capture Reveals ZNF423 and CEP164 Mutations, Linking Renal Ciliopathies to DNA Damage Response Signaling. *Cell*, 150, 533-548.

77 Zhou, W., Otto, E.A., Cluckey, A., Airik, R., Hurd, T.W., Chaki, M., Diaz, K., Lach, F.P., Bennett, G.R., Gee, H.Y. *et al.* (2012) FAN1 mutations cause karyomegalic interstitial nephritis, linking chronic kidney failure to defective DNA damage repair. *Nat Genet*, 44, 910-915.

78 Airik, R., Slaats, G.G., Guo, Z., Weiss, A.-C., Khan, N., Ghosh, A., Hurd, T.W., Bekker-Jensen, S., Schrøder, J.M., Elledge, S.J. *et al.* (2014) Renal-Retinal Ciliopathy Gene Sdccag8 Regulates DNA Damage Response Signaling. *Journal of the American Society of Nephrology*, 25, 2573-2583.

79 Slaats, G.G., Ghosh, A.K., Falke, L.L., Le Corre, S., Shaltiel, I.A., van de Hoek, G., Klasson, T.D., Stokman, M.F., Logister, I., Verhaar, M.C. *et al.* (2014) Nephronophthisis-Associated CEP164 Regulates Cell Cycle Progression, Apoptosis and Epithelial-to-Mesenchymal Transition. *PLoS Genet*, 10, e1004594.

80 Slaats, G.G., Saldivar, J.C., Bacal, J., Zeman, M.K., Kile, A.C., Hynes, A.M., Srivastava, S., Nazmutdinova, J., Ouden, K.d., Zagers, M.S. *et al.* (2015) DNA replication stress underlies renal phenotypes in CEP290-associated Joubert syndrome. *The Journal of Clinical Investigation*, 125, 3657-3666.

81 Choi, Hyo Jei C., Lin, J.-R., Vannier, J.-B., Slaats, Gisela G., Kile, Andrew C., Paulsen, Renee D., Manning, Danielle K., Beier, David R., Giles, Rachel H., Boulton, Simon J. *et al.* (2013) NEK8 Links the ATR-Regulated Replication Stress Response and S Phase CDK Activity to Renal Ciliopathies. *Molecular Cell*, 51, 423-439.

82 Slaats, G.G. and Giles, R.H. (2015) Are renal ciliopathies (replication) stressed out? *Trends in Cell Biology*, 25, 317-319.

83 O'Driscoll, M. (2012) Diseases Associated with Defective Responses to DNA Damage. *Cold Spring Harbor Perspectives in Biology*, 4.

84 Alcantara, D. and O'Driscoll, M. (2014) Congenital microcephaly. *American Journal of Medical Genetics Part C: Seminars in Medical Genetics*, 166, 124-139.

85 Lavin, M.F. (2008) Ataxia-telangiectasia: from a rare disorder to a paradigm for cell signalling and cancer. *Nat Rev Mol Cell Biol*, 9, 759-769.

86 Shiloh, Y. and Ziv, Y. (2013) The ATM protein kinase: regulating the cellular response to genotoxic stress, and more. *Nat Rev Mol Cell Biol*, 14, 197-210.

87 Coene, K., Roepman, R., Doherty, D., Afroze, B., Kroes, H., Letteboer, S., Ngu, L., Budny, B., van Wijk, E., Gorden, N. *et al.* (2009) OFD1 is mutated in X-linked Joubert syndrome and interacts with LCA5-encoded lebercilin. *Am J Hum Genet*, 85, 465 - 481.

88 Otto, E.A., Hurd, T.W., Airik, R., Chaki, M., Zhou, W., Stoetzel, C., Patil, S.B., Levy, S., Ghosh, A.K., Murga-Zamalloa, C.A. *et al.* (2010) Candidate exome capture identifies mutation of SDCCAG8 as the cause of a retinal-renal ciliopathy. *Nat Genet*, 42, 840-850.

89 Toriyama, M., Lee, C., Taylor, S.P., Duran, I., Cohn, D.H., Bruel, A.-L., Tabler, J.M., Drew, K., Kelly, M.R., Kim, S. *et al.* (2016) The ciliopathy-associated CPLANE proteins direct basal body recruitment of intraflagellar transport machinery. *Nat Genet*, 48, 648-656.

90 Bjornsson, H.T., Benjamin, J.S., Zhang, L., Weissman, J., Gerber, E.E., Chen, Y.-C., Vaurio, R.G., Potter, M.C., Hansen, K.D. and Dietz, H.C. (2014) Histone deacetylase inhibition rescues structural and functional brain deficits in a mouse model of Kabuki syndrome. *Science Translational Medicine*, 6, 256ra135-256ra135.

91 Fraga, M.F., Ballestar, E., Villar-Garea, A., Boix-Chornet, M., Espada, J., Schotta, G., Bonaldi, T., Haydon, C., Ropero, S., Petrie, K. *et al.* (2005) Loss of acetylation at Lys16 and trimethylation at Lys20 of histone H4 is a common hallmark of human cancer. *Nat Genet*, 37, 391-400.

92 Gorrini, C., Squatrito, M., Luise, C., Syed, N., Perna, D., Wark, L., Martinato, F., Sardella, D., Verrecchia, A., Bennett, S. *et al.* (2007) Tip60 is a haplo-insufficient tumour suppressor required for an oncogene-induced DNA damage response. *Nature*, 448, 1063-1067.

93 Lobrich, M. and Jeggo, P.A. (2007) The impact of a negligent G2/M checkpoint on genomic instability and cancer induction. *Nat Rev Cancer*, 7, 861-869.

94 Deckbar, D., Birraux, J., Krempler, A., Tchouandong, L., Beucher, A., Walker, S., Stiff, T., Jeggo, P. and Lobrich, M. (2007) Chromosome breakage after G2 checkpoint release. *J. Cell Biol.*, 176, 749-755.

95 Dehay, C. and Kennedy, H. (2007) Cell-cycle control and cortical development. *Nat Rev Neurosci*, 8, 438-450.

96 Gatz, S.A., Ju, L., Gruber, R., Hoffmann, E., Carr, A.M., Wang, Z.-Q., Liu, C. and Jeggo, P.A. (2011) Requirement for DNA Ligase IV during Embryonic Neuronal Development. *The Journal of Neuroscience*, 31, 10088-10100.

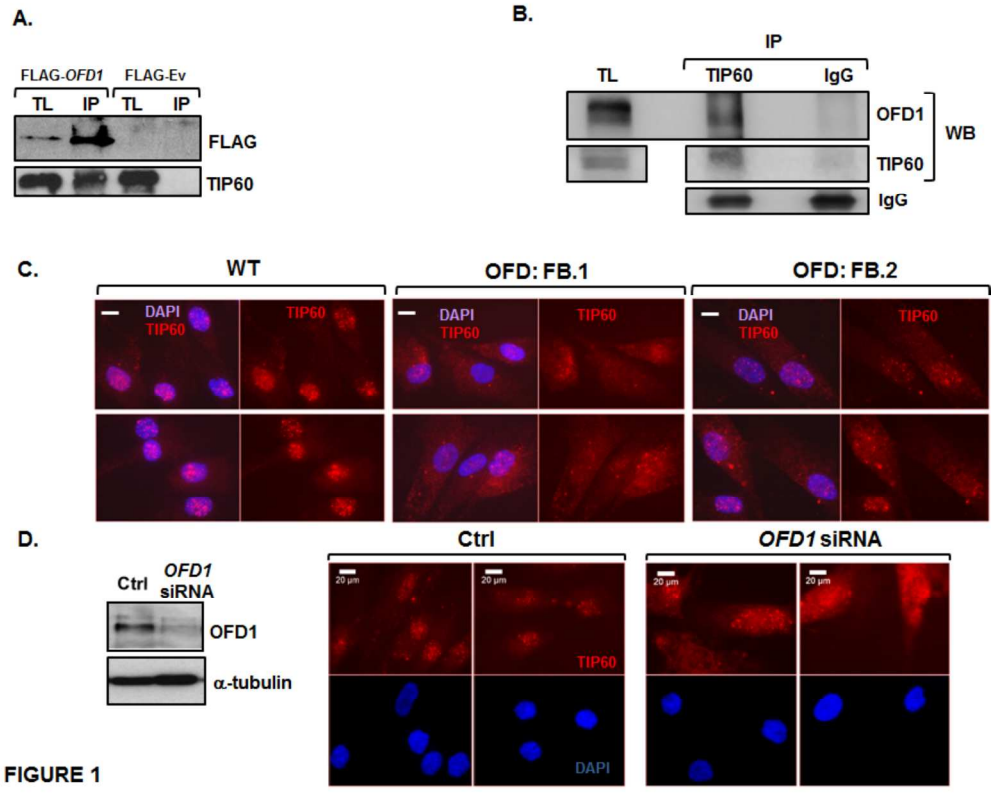

FIGURE 1

FIG 1

256x206mm (300 x 300 DPI)

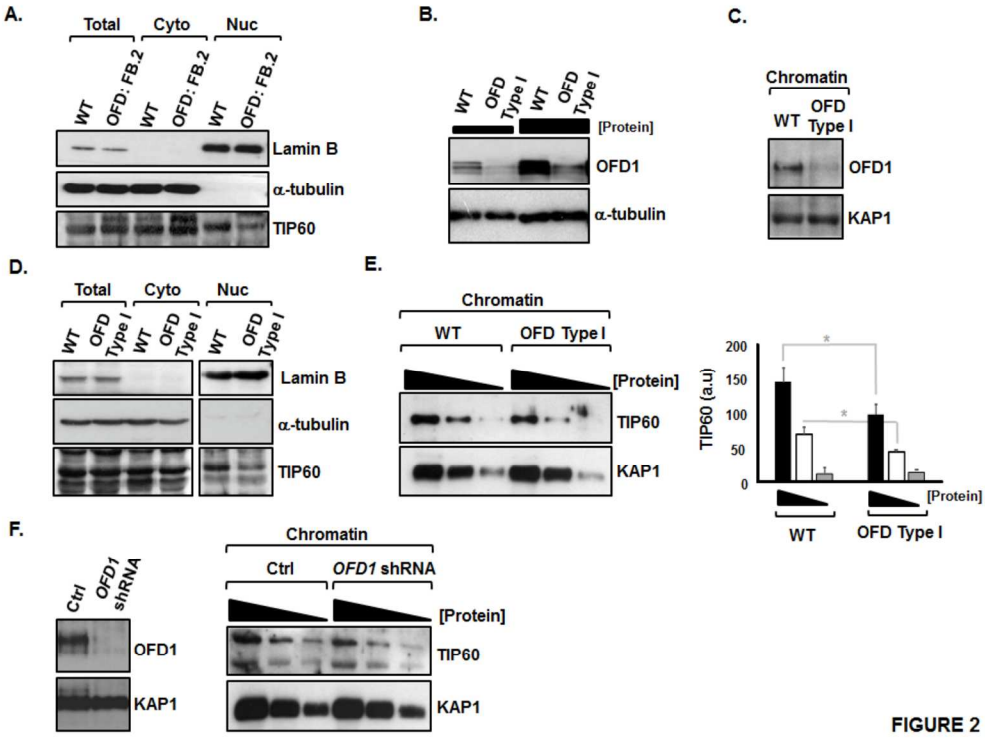

FIGURE 2

FIG 2

271x204mm (300 x 300 DPI)

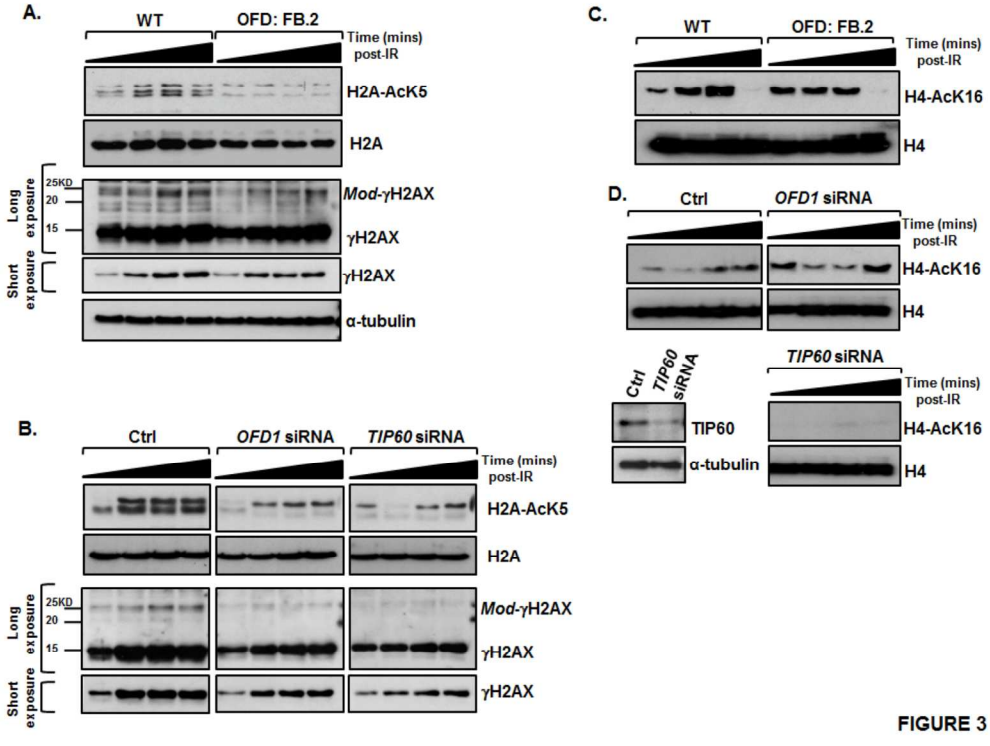

FIGURE 3

FIG 3

274x207mm (300 x 300 DPI)

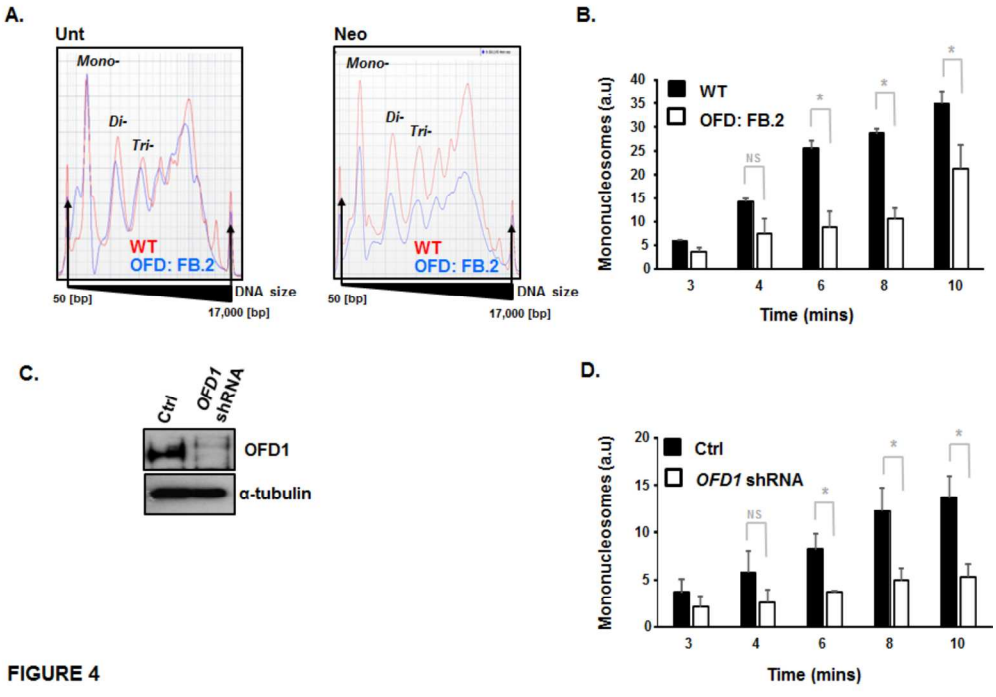

FIGURE 4

FIG 4

290x203mm (300 x 300 DPI)

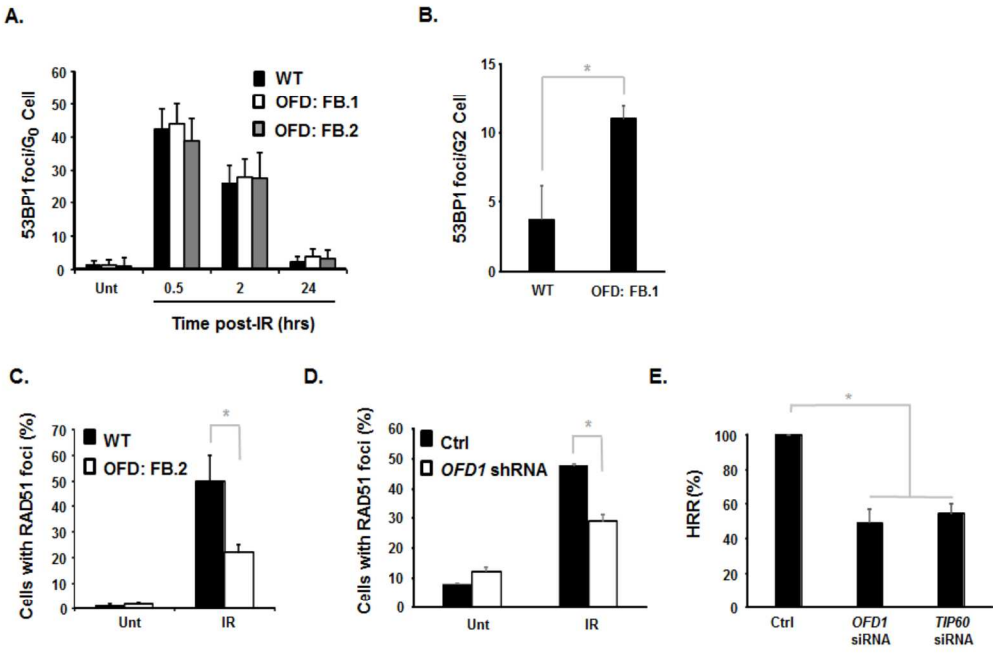

FIGURE 5

FIG 5

290x204mm (300 x 300 DPI)

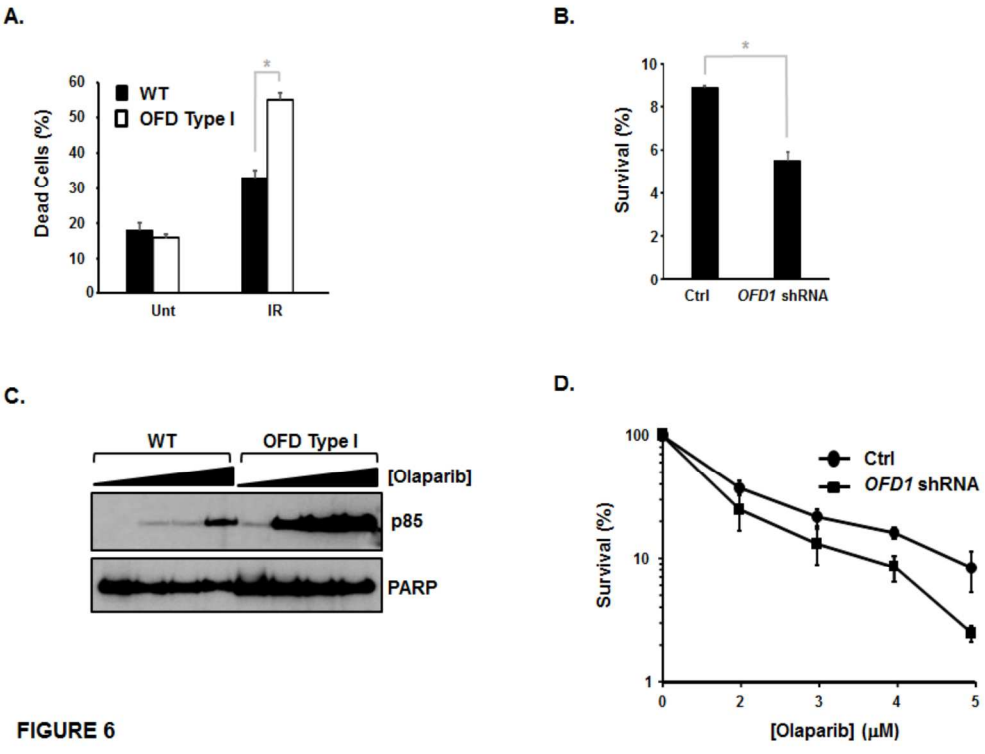

FIGURE 6

FIG 6

272x207mm (300 x 300 DPI)

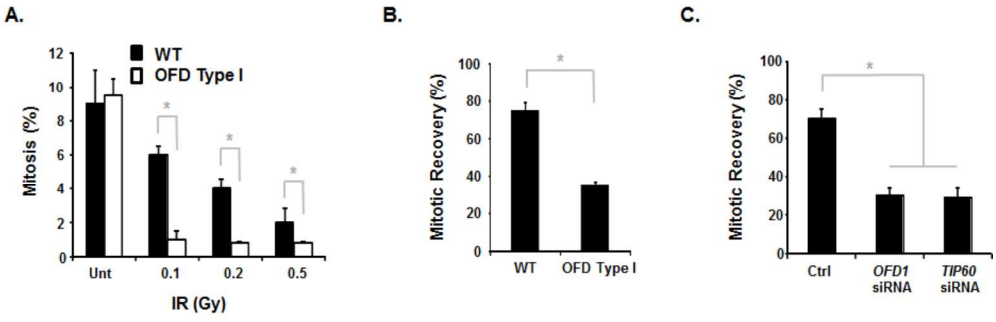

FIGURE 7

FIG 7

290x109mm (300 x 300 DPI)